4D Printing MOF-derivate/Multi-fluorination Nanocomposites for Ultra-Efficient Electromagnetic Wave Absorption and Robust Environmentally Adaptive

Kun Li[1], *Liuwenlin Han*[1], *Tiancheng Wang*[2], *Junying Zhang*[1]*, *Jue Cheng*[1]*

1. Key Laboratory of Carbon Fiber and Functional Polymers, Ministry of Education, Beijing University of Chemical Technology, Beijing 100029, P.R. China.

2. Department of Chemical and Biomolecular Engineering, University of Pennsylvania, Philadelphia, PA 19104, USA

*Corresponding author: Prof. *Junying Zhang* & Prof. *Jue. Cheng*

Tel: +86-10-64425439; E-mail: zhangjy@mail.buct.edu.cn (J.Y. Zhang); chengjue@mail.buct.edu.cn (. J. Cheng)

Supplementary Material

Experiment Section

1. MATERIALS AND METHODS

1.1 Materials

1H, 1H, 2H, 2H-Perfluorodexthiol (95%), Dially bisphenol A (99%), 2-hydroxy-2-methylpropiophenone (1173, 98%), Tetra methyl ammonium bromide (TMAB, 97%) and epoxy chloropropane (ECH, 95%) were supplied by Beijing MREDA Technology Co., Ltd. Lithium fluoride (LiF), hydrochloric acid (HCl), 2,4,6,8-Tetravinyl-2,4,6,8-tetramethylcyclotetrasiloxane (V4), octamethyl cyclotetrasiloxane (D4), tetramethylammonium hydroxide (TMAH) and tetramethyl-1,3-bis(3-aminopropyl)disiloxane were purchased from Beijing HongHu Technology Co., Ltd. Ti_3AlC_2 and Carboxylated CNTs (COOH@CNTs) were purchased from XianFeng Nano Material Technology Co., Ltd. $Co(NO_3)_2{\cdot}6H_2O$ (90%), 2-methylimidazole (2-Im, 95%), $Ni(NO_3)_2{\cdot}6H_2O$ (95%), 2,4,6-Tris(dimethylaminomethyl)phenol (DMP-30), and benzene-1,3,5-tricarboxylic acid (H_3BTC) were purchased from Sinopharm Chemical Reagent Co., Ltd.

1.2 Synthesis of F8EP

First, Dially bisphenol A (30.8g, 0.1mol), epichlorohydrin (92.5g, 1mol) and NaOH (14.4g, 0.36mol) were mixed by a mechanical stirring for 50 min in 250 ml round-bottomed flask at 55 ^{o}C. Then, TMAB (0.245 g, 0.0016 mol) was added and the temperature was maintained at 68-75 ^{o}C for another 5 h. The DADGEBA was washed with deionized water until the pH was 7, and the residual solvent was removed by rotating evaporator. The DADGEBA, 1H, 1H, 2H, 2H-Perfluorodexthiol (S-H:C=C was 1:1) and 1173 (initiator, 0.5% mass ratio) were mixed for UV light-emitting diode (365 nm) for 60 min. Finally, the epoxy value of F8EP (0.431mol/100g) was determined by the hydrochloric acid-acetone method.

1.3 Synthesis of F8-ATPS

V-ATPS: D4 (58.9g), V4 (7.6g), tetramethyl-1,3-bis(3-aminopropyl)disiloxane (18.3g) and TMAH (0.04g) were added into a three-neck flask with a stir paddle and condenser under nitrogen atmosphere. The mixture was stirred for 4 h at 100 °C, then heated to 120 °C for 1 h, and then heated to 150 °C for 30 min to decompose the catalyst TMAH. The decomposing products of TMAH (mainly trimethylamine, methanol) unreacted D4 and V4, and low-molecular weight products were removed at 170 °C in vacuum.

F8-ATPS: The V-ATPS, 1H, 1H, 2H, 2H-Perfluorodexthiol (S-H:C=C was 1:1) and 1173 (initiator, 0.5% mass ratio) were mixed for UV light-emitting diode (365 nm) for 90 min.

1.4 Synthesis of MXene

Initially, dissolving 1g LiF powder in 20 mL 9 M HCl solution, and the mixture was stirred for a few minutes until all LiF particles were dissolved in the HCl solution. The etching container was put in an ice bath and 1 g of Ti_3AlC_2 powder was slowly added to the etching mixture to avoid excessive heat generation. Then, the etching process was continued at 35 ^{o}C for 24 h while the solution was stirred at 500 rpm. Afterward, the acidic suspension was washed, collected, and dried. Then, the freeze-dried product was dissolved in water and sonicated for 40 min. Finally, the mixed solution was centrifuged at a speed of 3500 rpm for 1 h to collect the MXene ($Ti_3C_2T_x$) supernatant.

1.5 Synthesis of CoMXene

The strategy for the preparation of CoMXene was illustrated in Scheme 1, 0.2g of $Co(NO_3)_2 \cdot 6H_2O$ and 0.1g of MXene were added into 30ml methanol with vigorously stirring and ultrasound to obtain a homogeneous dispersion. And the 0.42g of 2-Im was fully dissolved in 30ml methanol with stirring. Then, the above solutions were mixed into the flask, the obtained dark purple solution after stirring 60min was aged in 35 ℃ for 24 h. The sediment product was separated after centrifuging at 7000 rpm and washed with methanol for five times. At last, the ZiF67@MXene precipitates were dried at 60 ^oC for 24h, and the product was annealed at 800 ^oC for 3h in argon to obtain the CoMXene magnetic powder.

1.6 Synthesis of CoNiCNT

The strategy for the preparation of CoNiCNT was illustrated in Scheme 1, 0.2g of $Co(NO_3)_2 \cdot 6H_2O$ and 0.1g of COOH@CNTs were added into 30ml methanol with vigorously stirring and ultrasound to obtain a homogeneous dispersion. And the 0.42g of 2-Im was fully dissolved in 30ml methanol with stirring. Then, the above solutions were mixed into the flask, the obtained dark purple solution after stirring 60min was aged in 35 ℃ for 24 h. The sediment product was separated after centrifuging at 7000 rpm and washed with methanol for five times. At last, the ZiF67-COOH@CNT precipitates were dried at 60 ^oC for 24h. 0.22g of ZiF67-COOH@CNT and 0.2g of H_3BTC were added into 35 ml DMF, which was mixed by a stirring and ultrasound for 120 min. Then, the mixture was transferred into 50ml Teflon-lined autoclave and heated at 150 ^oC for 12h. The sediment product was separated after centrifuging at 6000 rpm and washed with deionized water for five times. At last, the CoNi-COOH@CNT precipitates were dried at 80 ^oC for 24h, and the product was annealed at 800 ^oC for 3h in argon to obtain the CoNiCNT magnetic powder.

1.7 Preparation of F8EP-FSi and CoM@CoNiC-F

F8EP-FSi: The F8-ATPS and F8EP were quickly mixed in the mass ratios of 129.3/100 at 90 ^oC, and then 0.5% wt DMP-30 was added into the mixtures. After mixing well, the final mixture was cured at 120 ^oC for 3h, followed by 150 ^oC for 4h. The cured sample was named F8EP-FSi.

3D Printing of CoM@CoNiC-F nanocomposite: The CoM@CoNiC-F suspensions were prepared by mixing CoMXene, CoNiCNT, F8-ATPS, F8EP and DMP-30 (mass ratio was 4.59/6.88/9.17/11.46/13.76: 9.18/13.76/18.34/22.92/27.52: 100: 129.3: 1.146), and subjected to ultrasound in an ice bath for 2 h to obtain stable prinking-inks. The optimal parameters for DIW printing are layer of 0.5mm, extrusion speed of 10mm/s and printing speed of 15mm/s. After printing, the objects are cured at 120 W for 20 min, 180 W for 40 min, and 220 W for 30 min in microwave irradiation reactor. Accordingly, the cured 3D-printed sample was named X CoM@CoNiC-F nanocomposite, and the X (6, 9, 12, 15, 18) is representing the mass ratio of CoMXene: CoNiCNT: F8EP-FSi mixture of X/3: 2X/3: 100.

Besides, 12 CoMXene-F and 12 CoNiCNT-F nanocomposites were prepared as control samples by the same procedure.

1.8 Characterization

^{1}H, ^{13}C and ^{19}F NMR spectra were recorded on Bruker DPX-600 spectrometer ($CDCl_3$). FTIR spectra were measured by absorbance mode ranging from 4000 to 500 cm^{-1} conducted on Nicolet Nexus 670 spectrometer. Nitrogen adsorption-desorption isotherm measurements were carried out with adsorption analyzer (ASAP-2460, Micromeritics) for the specific surface area and pore size distribution of samples. X-ray photoelectron spectroscopy (XPS) was recorded with Thermo Scientific. X-ray diffraction (XRD) was D8-Advance, Bruker. Raman spectrum was tested on a confocal Raman spectrometer (LabRam ARAMIS). The viscosity and moduli curves of inks were obtained by Rotary rheometer (Anton Paar MCR101). Thermomechanical properties were performed on Dynamic Mechanical Analysis (DMA, TA Instruments Q800) at a heating rate of 5 °C/min. Tensile strength was tested by Universal Materials Testing Machine (MTS CMT4204, GB/T 1040.2-2006). Thermogravimetric analyzer (TGA, TA Instruments Q600) was performed at a heating rate of 10 °C/min under the condition of N_2 flow (50 mL/min). The micromorphology of specimens was observed by a JSM-7800F field emission scanning electron microscope (SEM) with an energy dispersive spectrometer (EDS) and a transmission electron microscope (TEM, JEM-100CX, JEOL). The micro/nano scale feature was obtained by using Atomic Force Microscope (AFM, DMFASTSCAN2-SYS). The contact angles (CAs) measurement was conducted by using a Drop Shape Analysis System DSA10-MK2. The

electromagnetic parameters were analyzed using vector network analyzer (N5244A, Agilent), and all samples were fabricated into coaxial rings. Electrochemical impedance spectroscopy (EIS) and potentiodynamic polarization tests (three-electrode system, Autolab Potentiostat/Galvanostat Model PGSTAT 302N) were used to investigate the corrosion resistance of the samples in 3.5 wt. % NaCl solution. The cone calorimeter test was measured by an FTT cone calorimeter, and the heat flux was 35 kW/m^2. The LOI was determined on an HC-2 LOI digital oxygen index instrument (China) based on ASTM D2863 and UL-94, and vertical burning level tests were performed using a CFZ-2 Horizontal-Vertical-Tester (China) according to ASTM D3801-19.

Supplementary Figures

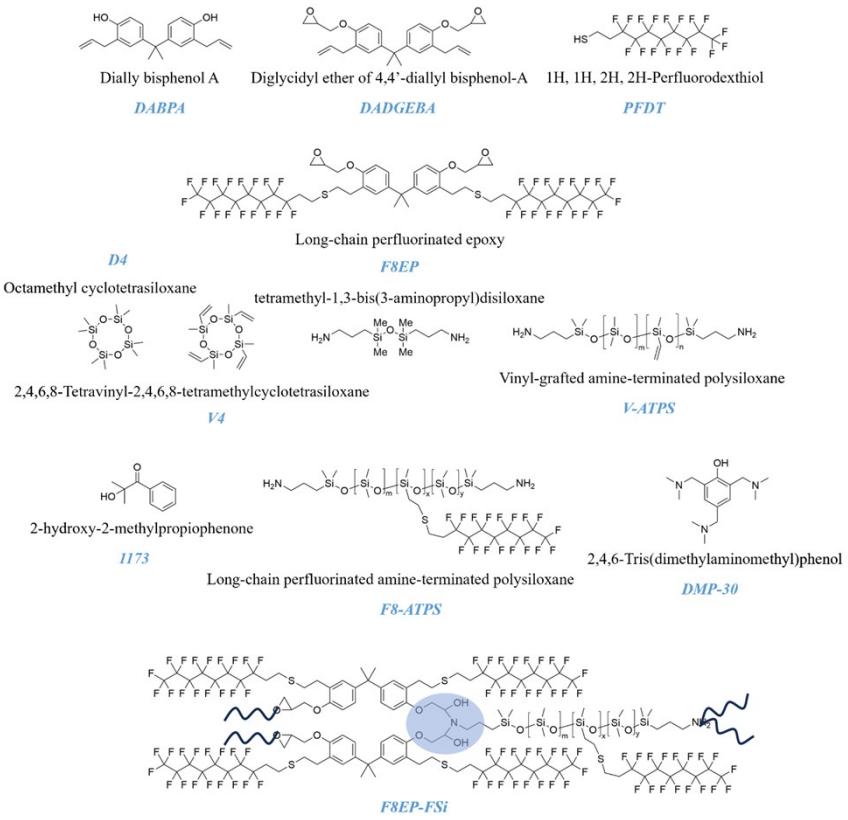

Fig S1. The detailed structure and abbreviation of all component.

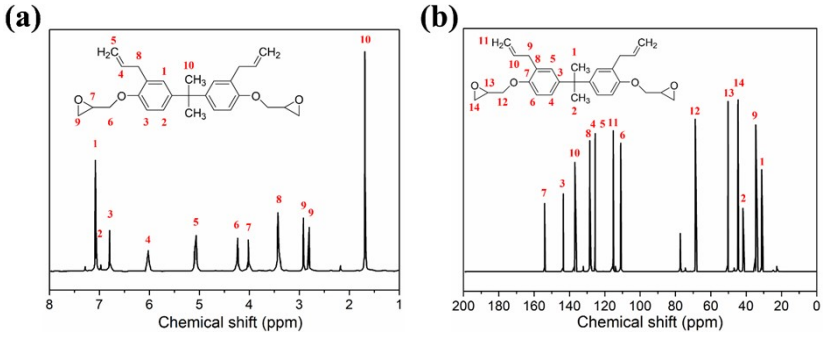

Fig S2. (a) ^{1}H NMR and (b) ^{13}C NMR spectra of DADGEBA.

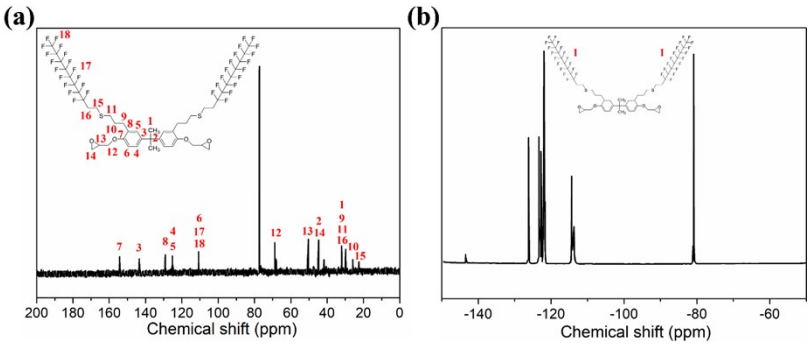

Fig S3. (a) ^{13}C NMR spectra and (b) ^{19}F NMR spectra of F8EP.

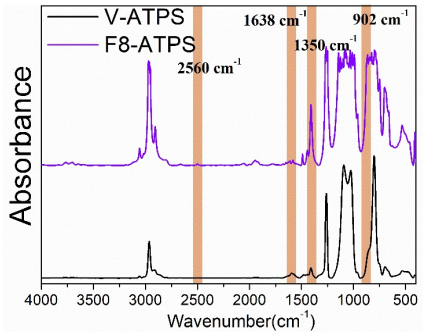

Fig S4. FTIR spectrum of V-ATPS and F8-ATPS.

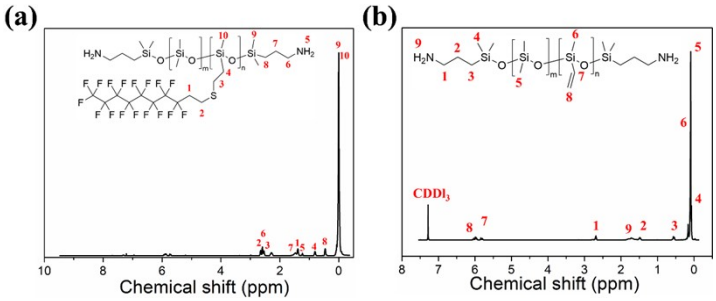

Fig S5. ^{1}H NMR spectrum of (a) F8-ATPS and (b) V-ATPS.

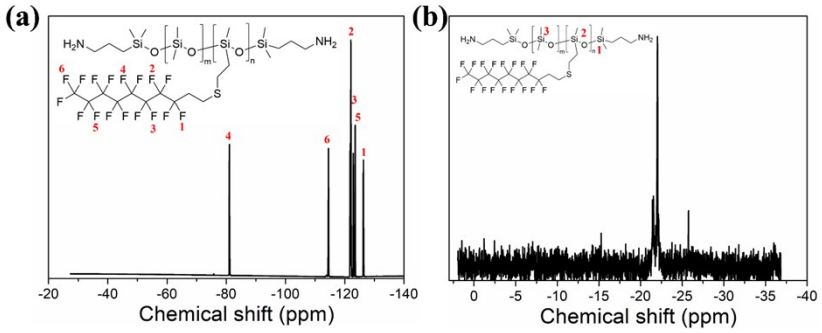

Fig S6. (a) ^{29}Si NMR and ^{19}F NMR spectrum of F8-ATPS.

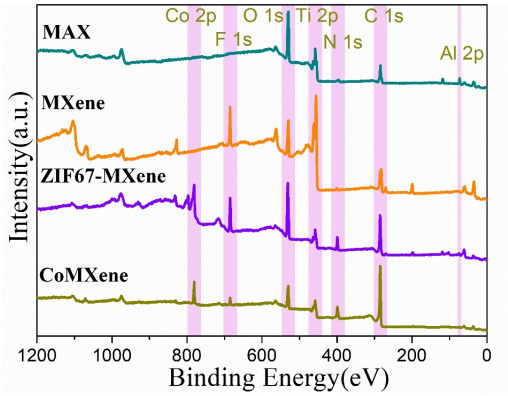

Fig S7. XPS spectrum of CoMXene.

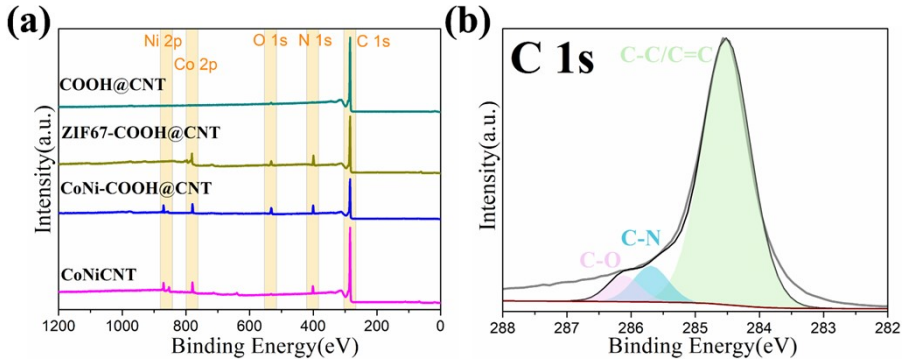

Fig S8. (a) XPS spectrum and (b) high-resolution C 1s spectrum of CoNiCNT.

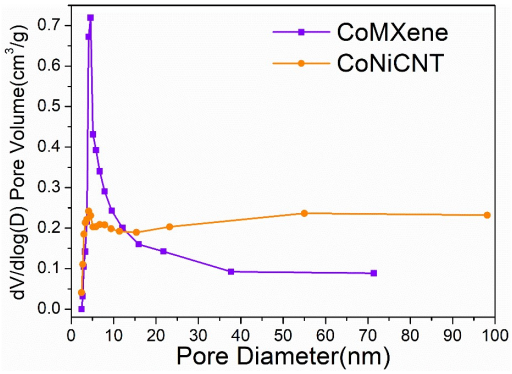

Fig S9. Pore size distribution of CoMXene and CoNiCNT.

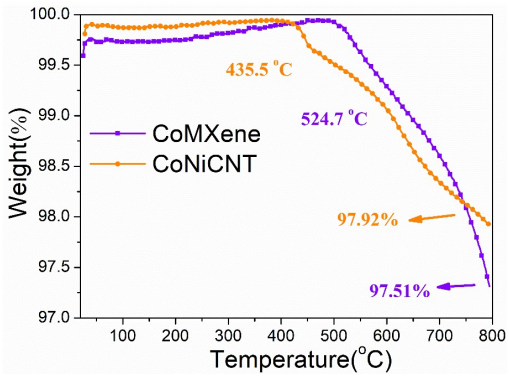

1

2 Fig S10. TGA curve of CoMXene and CoNiCNT.

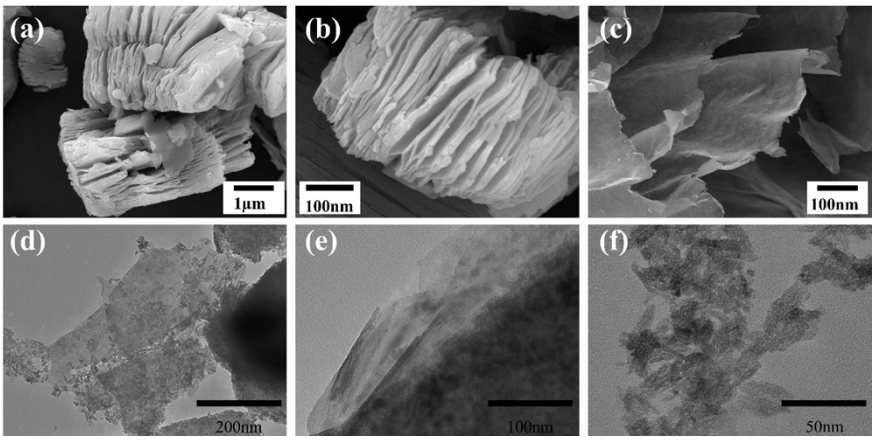

3

4 Fig S11. (a, b) SEM of accordion-like $Ti_3C_2T_x$, (c) SEM and (d, e, f) TEM of single-flake $Ti_3C_2T_x$.

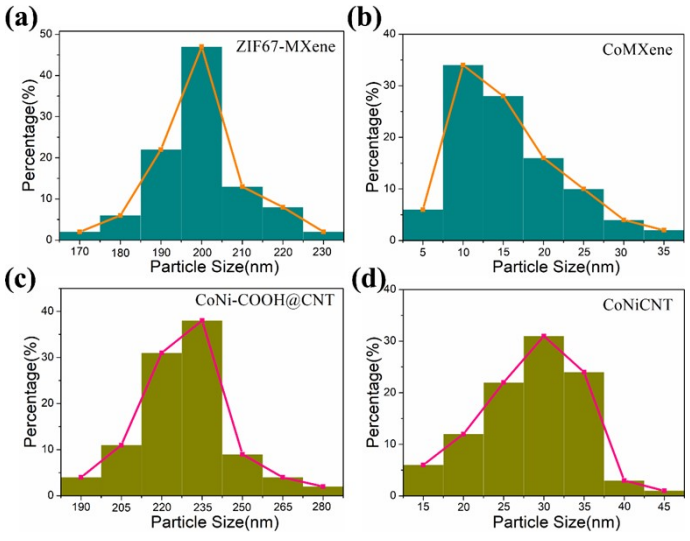

5

6 Fig S12. Corresponding particle size distribution charts of (a) ZIF67-MXene, (b) CoMXene, (c) CoNi-
7 COOH@CNT and (d) CoNiCNT.

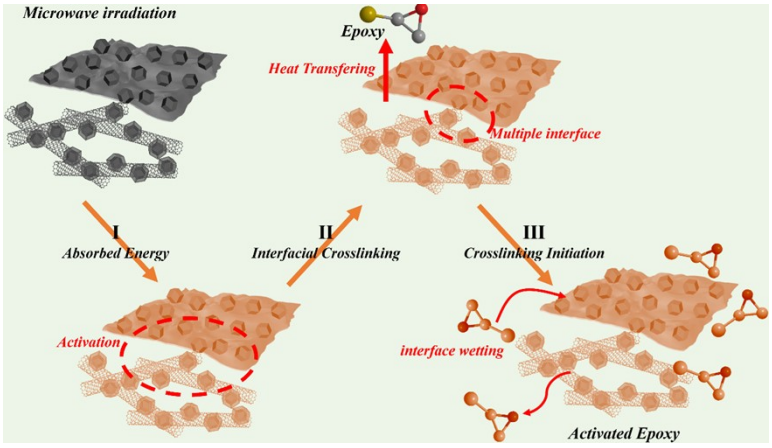

Fig S13. Schematic diagram of microwave effect.

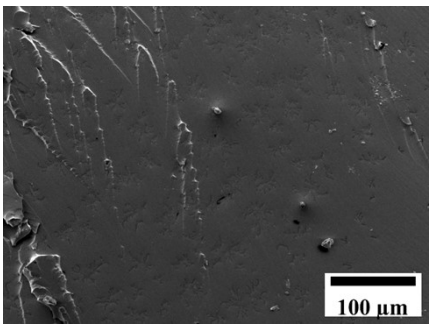

Fig S14. SEM of tensile fracture surface for FEP matrix.

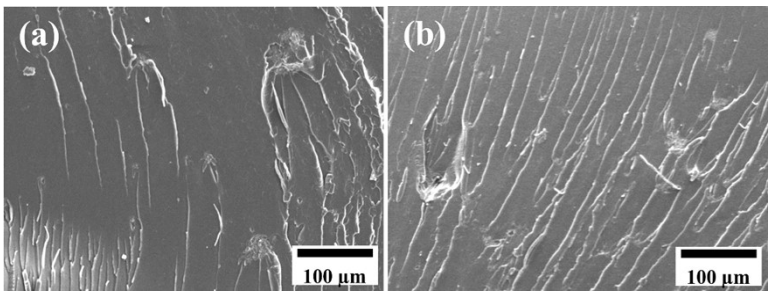

Fig S15. SEM of tensile fracture surface for (a) 6 CoM@CoNiC-F nanocomposites and (b) 9 CoM@CoNiC-F nanocomposites.

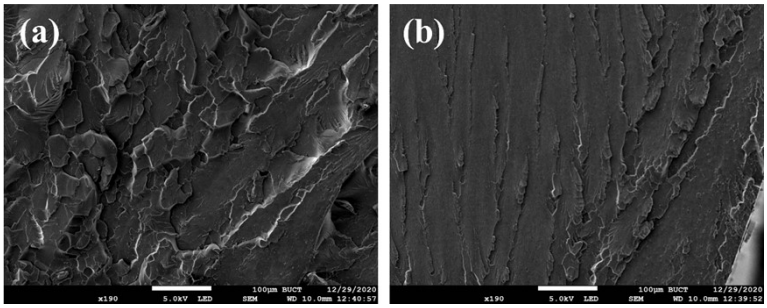

Fig S16. SEM of tensile fracture surface for (a) 12 CoM-F nanocomposites and (b) 12 CoNiCNT-F nanocomposites.

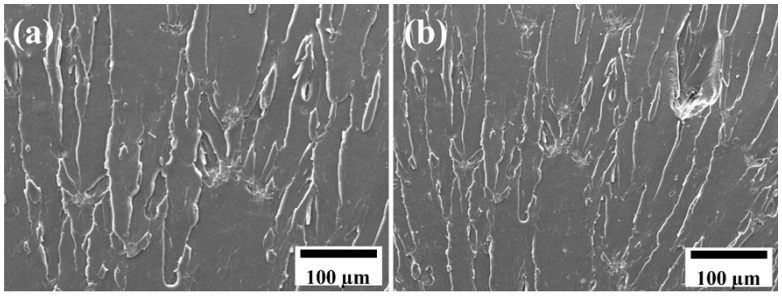

Fig S17. SEM of tensile fracture surface for (a) 15 CoM@CoNiC-F nanocomposites and (b) 18 CoM@CoNiC-F nanocomposites.

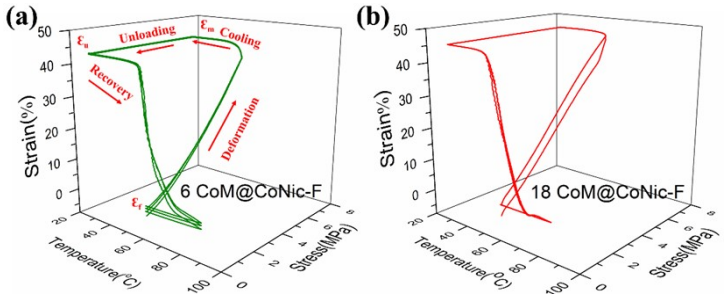

Fig S18. Three-dimensional strain-stress-temperature (45%) cycle diagrams for (a) 6 and (b) 18 CoM@CoNiC-F.

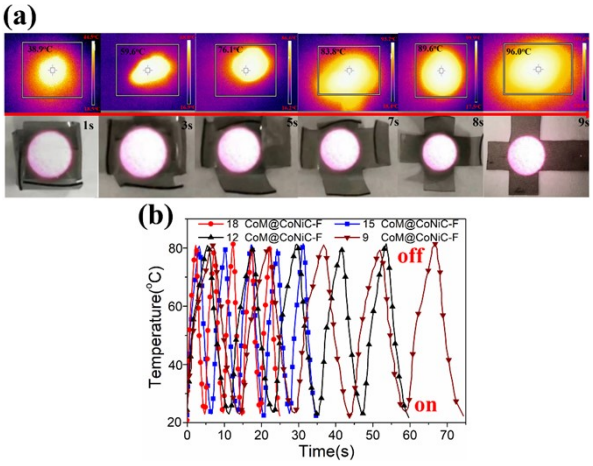

Fig S19. (a) photo induced shape memory of 6 CoM@CoNiC-F. (b) photothermal conversion effect of CoM@CoNiC-F nanocomposites.

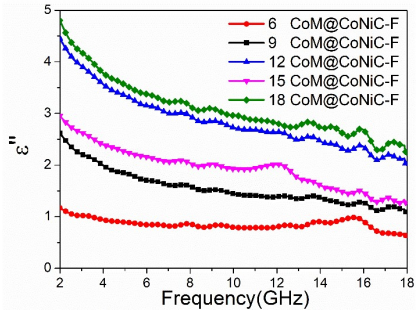

Fig S20. The ε'' curve of CoM@CoNiC-F nanocomposites.

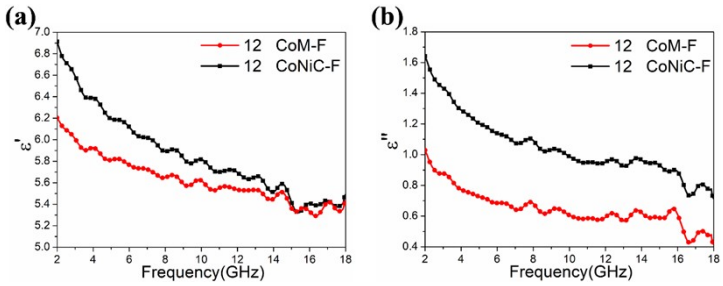

Fig S21. (a) ε' and (b) ε'' curve of 12 CoM-F and 12 CoNiCNT-F nanocomposites.

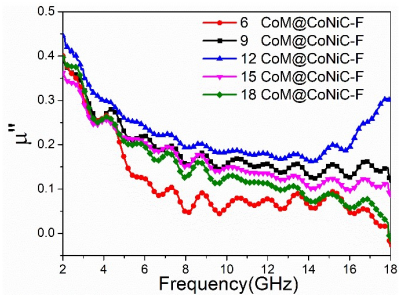

Fig S22. The μ'' curve of CoM@CoNiC-F nanocomposites.

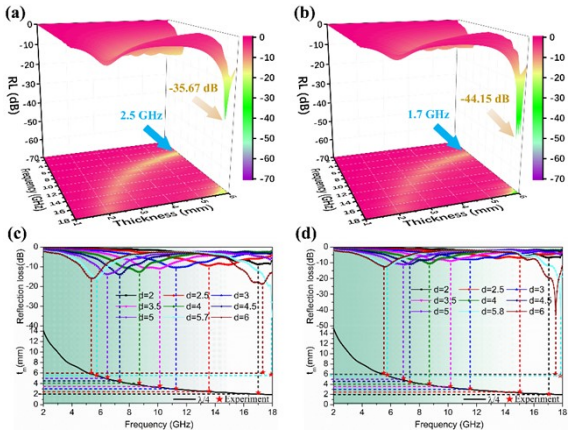

Fig S23. The 3D RL plots of (a) 12 CoM-F and (b) 12 CoNiCNT-F. The frequency dependance of RL on frequency at λ/4 thickness of (c) 12 CoM-F and (d) 12 CoNiCNT-F.

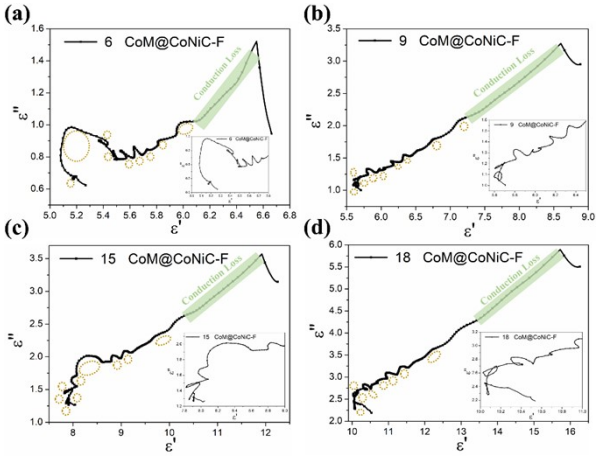

Fig S24. The Cole-Cole semicircles of (a) 6 CoM@CoNiC-F, (b) 9 CoM@CoNiC-F, (c) 15 CoM@CoNiC-F and (d) 18 CoM@CoNiC-F.

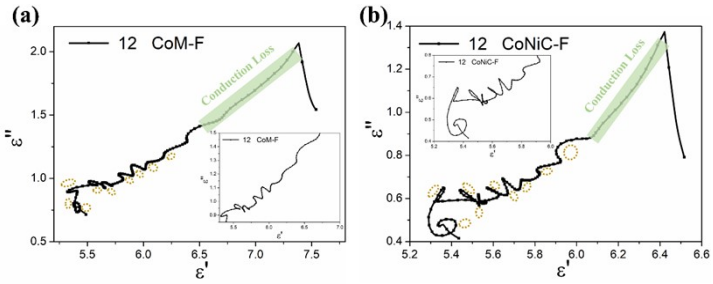

Fig S25. The Cole-Cole semicircles of (a) 12 CoM-F and (b) 12 CoNiCNT-F.

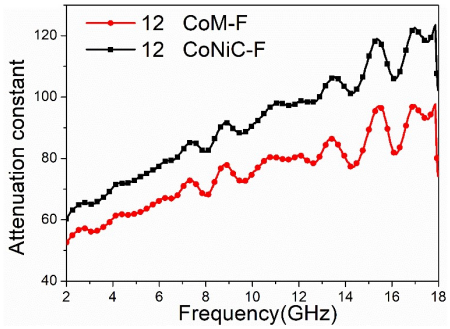

Fig S26. The attenuation constant curves of 12 CoM-F and 12 CoNiCNT-F.

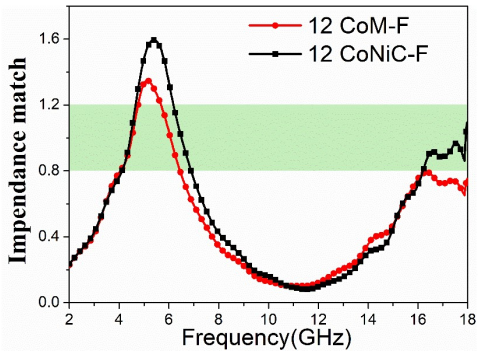

Fig S27. The impedance matching curves of 12 CoM-F and 12 CoNiCNT-F.

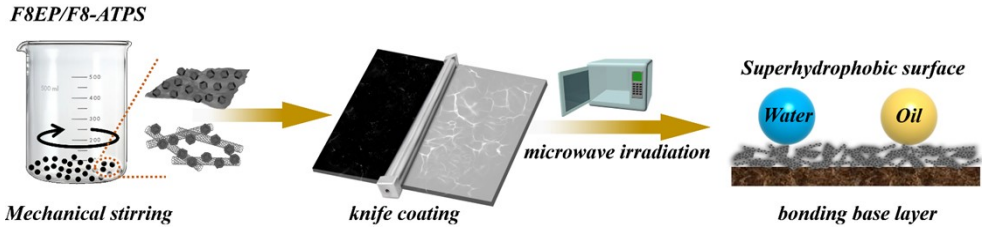

Fig S28. Schematic diagram of fabricating the CoM@CoNiC-F coatings.

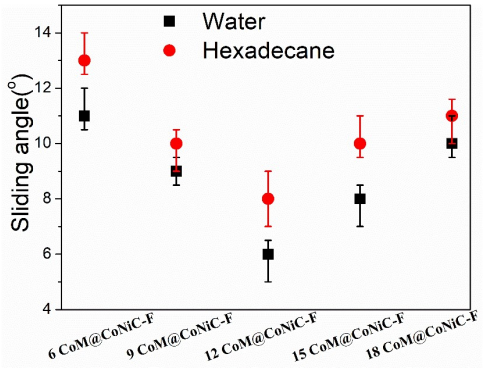

Fig S29. The sliding angle of CoM@CoNiC-F coatings.

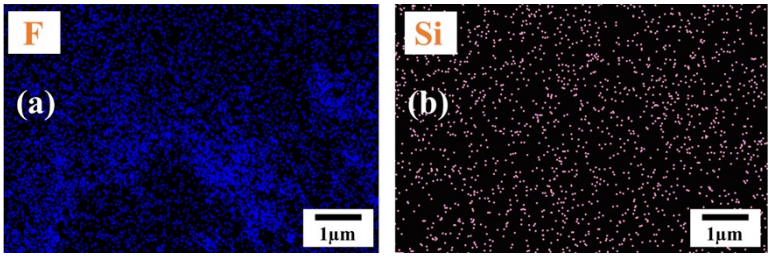

Fig S30. EDS images of (a) F and (b) Si element of 12 CoM@CoNiC-F coating surface.

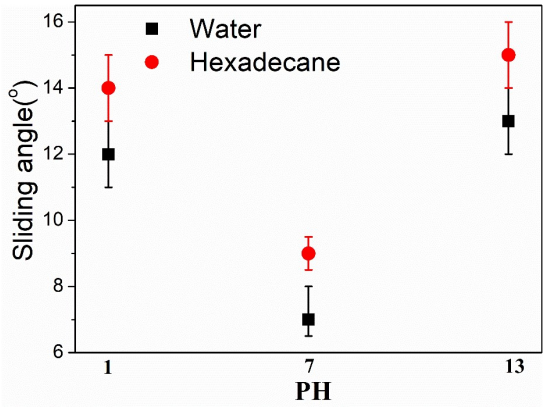

Fig S31. The sliding angle after corrosion in 0.1 M HCl, NaCl and aqueous solutions of 12 CoM@CoNiC-F coating.

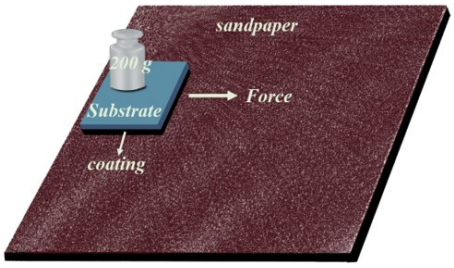

Fig S32. Schematic diagram of sandpaper abrasion.

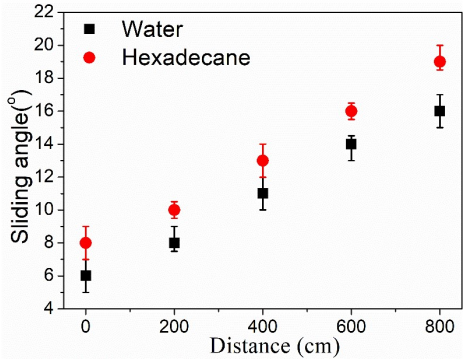

Fig S33. The sliding angle after different distance sandpaper abrasion of 12 CoM@CoNiC-F coating.

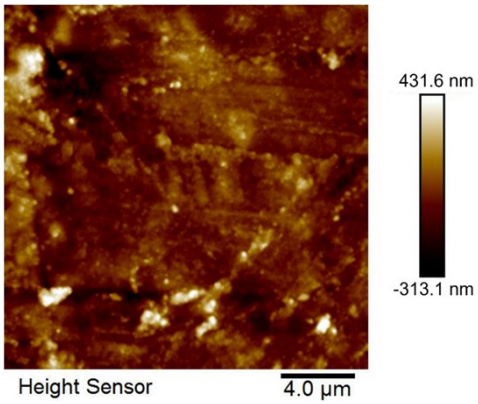

Fig S34. AFM height image after 800cm sandpaper abrasion of 12 CoM@CoNiC-F coating.

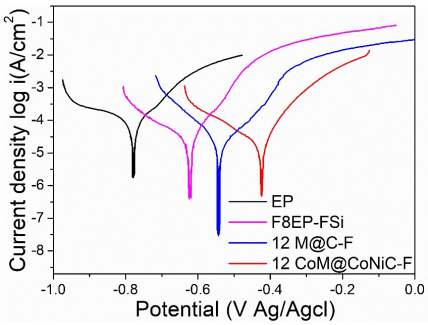

Fig S35. The Potentiodynamic polarization curves after 48 h immersion in NaCl solution.

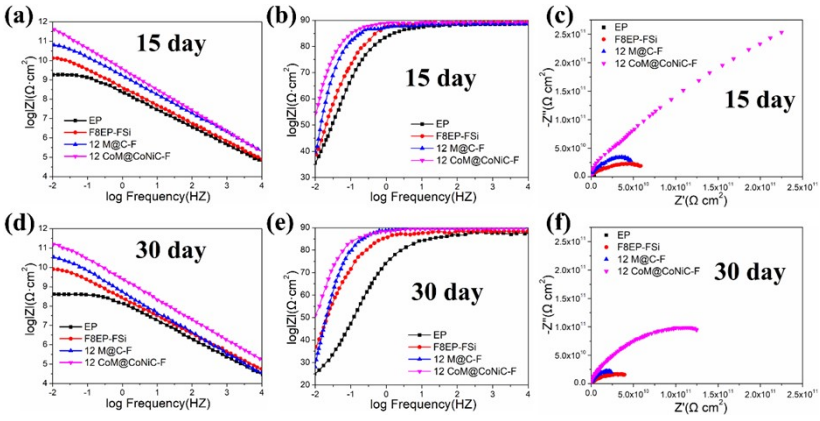

Fig S36. (a), (d) Bode-impedance, (b), (e) Bode-phase angle and (c), (f) Nyquist diagrams of different

coatings at 15, 30 days NaCl immersion.

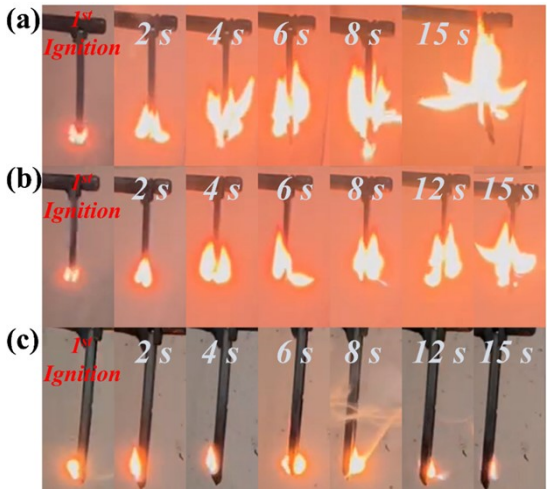

Fig S37. Vertical combustion images of (a) EP, (b) F8EP-FSi and (c) 12 M@C-F.

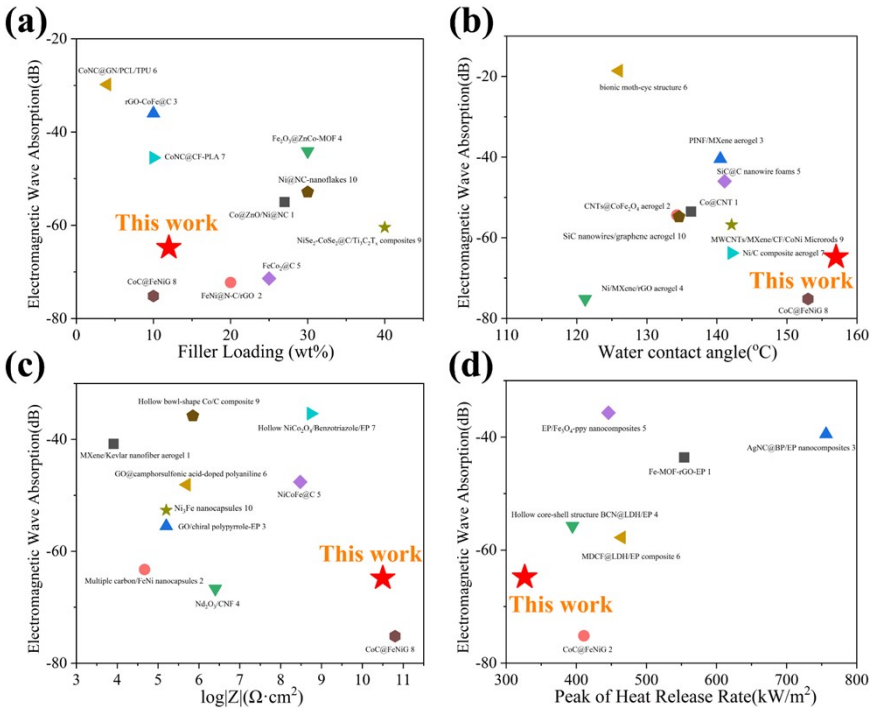

Fig S38. Comparison of (a) Filler loading, (b) water contact angle, (c) impedance modulus and (d) Peak of heat release rate and minimum reflection loss of literatures ever reported. The detailed information was presented in Table S1,2,3, 4 and reference.

Supplementary Tables

Table S1. Comparison of filler loading and EMW performance of literatures.

Material	Minimum	Filler Loading (%)

	reflection loss (dB)	
Co@ZnO/Ni@NC 1	-55	27
NiFe@N-C/rGO 2	-72.28	20
CNT-CoFe@C 3	-40.5	10
CoFe@ZnO@C 4	-44.13	30
FeM-alloy@C 5	-71.4	25
CoNC@GN/PCL/TPU 6	-29.8	4
CoNC@CF-PLA 7	--45.5	10
CoC@FeNiG 8	-75.18	10
$NiSe_2$-$CoSe_2$@C/$Ti_3C_2T_x$ 9	-60.46	40
Ni@NC-nf 10	-52.88	30
This work	-64.78	12

References

[1] Y. Cui, Z. Liu, X. Li, J. Ren, Y. Wang, Q. Zhang, B. Zhang, *Journal of Colloid and Interface Science* **2021**, 600, 99-110.

[2] H. Zhao, Q. Wang, H. Ma, Y. Zhao, L. Li, P. Li, J. Yan, J. Yun, W. Zhao, H. Zhang, Z. Zhang, C. Liu, *Carbon* **2023**, 201, 347-361.

[3] Y. Wang, H. Wang, J. Ye, L. Shi, X. Feng, *Chem. Eng. J.* **2020**, 383, 123096.

[4] M. Kong, X. Liu, Z. Jia, B. Wang, X. Wu, G. Wu, *Journal of Colloid and Interface Science* **2021**, 604, 39-51.

[5] L. Li, G. Li, W. Ouyang, Y. Zhang, F. Zeng, C. Liu, *Chem. Eng. J.* **2021**, 420, 127609.

[6] Y. Liu, X. Wei, X. He, J. Yao, R. Tan, P. Chen, B. Yao, J. Zhou, Z. Yao, *Adv. Funct. Mater.* **2023**, 33, 2211352

[7] T. Wu, X. Huan, X. Jia, G. Sui, L. Wu, Q. Cai, X. Yang, *Composites Part B* **2022**, 233, 109658.

[8] K. Li, L. Han, J. Zhang, J. Cheng, *Small Struct.* **2023**, 2300210.

[9] T. Hou, Z. Jia, B. Wang, H. Li, X. Liu, Q. Chi, G. Wu, *Chem. Eng. J.* **2021**, 422, 130079.

[10] L. Jin, P. Yi, L. Wan, J. Hou, P. Chen, J. Zu, B. Wei, Z. Yao, J. Zhou, *Chem. Eng. J.* **2022**, 427, 130940.

Table S2. Comparison of water contact angle and EMW performance of literatures.

Material	Minimum reflection loss (dB)	Water contact angle (°)
Co@CNT 1	-53.5	136.4
CNTs@$CoFe_2o_4$ aerogel 2	-54.4	134.3
PINF/MXene aerogel 3	-40.5	140.6
Ni/MXene/rGO aerogel 4	-75.2	121.2
SiC@C nanowire foams 5	-46.4	141.2
Bionic moth-eye structure 6	-18.8	126.4

Ni/C composite aerogel 7	-63.8	142.2
CoC@FeNiG 8	-75.18	153
MWCNTs/MXene/CF/CoNi Microrods 9	-56.8	142.1
Si nanowires/graphene aerogel10	-54.8	134.7
This work	-64.78	157

References

[1] B. Jiang, W. Yang, C. Wang, H. Bai, G. Ma, Z.Li, C. Zhang, S. Li, N. Chen, N. Ta, X. Wang, Y. Li, *Carbon* **2023**, 202, 173-186.

[2] J. Luo, Y. Wang, Z. Qu, W. Wang, D. Yu, *Chem. Eng. J.* **2022**, 442, 136388.

[3] L. Pu, Y. Liu, L. Li, C. Zhang, P. Ma, W. Dong, Y. Huang, T. Liu, *ACS Appl. Mater. Interfaces* **2021**, 13, 47134-47146.

[4] L. Liang, Q. Li, X. Yan, Y. Feng, Y. Wang, H. Zhang, X. Zhou, C. Liu, C. Shen, X. Xie, *ACS Nano* **2021**, 15, 6622-6632.

[5] Z. Cai, L. Su, H. Wang, M. Niu, H. Gao, D. Lu, M. Li, *ACS Appl. Mater. Interfaces* **2020**, 12, 8555-8562.

[6] L. Huang, Y. Duan, X. Dai, Y. Zeng, G. Ma, Y. Liu, S. Gao, W. Zhang, *Small* **2019**, 15, 1902730.

[7] P. Wang, L. Gai, B. Hu, Y. Liu, F. Wang, P. Xu, X. Han, Y. Du, *Carbon* **2023**, 212, 118132.

[8] K. Li, L. Han, J. Zhang, J. Cheng, *Small Struct.* **2023**, 2300210.

[9] B. Wang, Z. Xu, H. Wu, W. Nie, F. Huang, S. Li, H. Zhang, *Carbon* **2023**, 208, 50-59.

[10] Y. Cheng, M. Tan, P. Hu, X. Zhang, B. Sun, L. Yan, S. Zhou, W. Han, *Applied Surface Science* **2018**, 448, 138-144.

Table S3. Comparison of impedance modulus and EMW performance of literatures.

Material	**Minimum reflection loss (dB)**	**Impedance modulus (Ω·cm²)**
MXene/Kevlar nanofiber aerogel 1	-40.8	3.91
Multiple carbon/FeNi nanocapsules 2	-63.26	4.67
GO/chiral polypyrrole-EP 3	-55.5	5.22
Nd_2O_3/CNF 4	-66.7	6.41
NiCoFe@C 5	-47.6	8.48
GO@camphorsulfonic acid-doped polyaniline 6	-48.1	5.71
Hollow $NiCo_2O_4$/Benzotriazole/EP 7	-35.39	8.74
CoC@FeNiG 8	-75.18	10.8
Hollow bowl-shape Co/C composite 9	-52.66	5.22
NiFe nanocapsules 10	-35.8	5.85
This work	-64.78	10.5

References

[1] D. Hu, Y. Jiang, X. Huang, *Composites: Part A* **2022**, 156, 106865.

[2] Z. Lei, Y. Song, M. Li, S. Li, D. Geng, W. Liu, Y. Cui, H. Jiang, S. Ma, Z. Zhang, *Journal of Alloys and Compounds* **2023**, 936, 168216.

[3] T. Chen, B. Wang, Z. Qi, Z. Guo, Y. Tian, F. Meng, *ACS Appl. Nano Mater.* **2022**, 5, 9780-9791.

[4] T. Liu, L. Huang, X. Wang, Y. Yuan, *ACS Appl. Electron. Mater.* **2022**, 4, 4982-4995.

[5] C. Zheng, M. Ning, Z. Zou, G. Lv, Q. Wu, J. Hou, Q. Man, R. Li, *Small* **2023**, 2208211.

[6] H. Wang, H. Ren, C. Jing, J. Li, Q. Zhou, F. Meng, *Composites Science and Technology* **2021**, 204, 108630.

[7] C. Ma, W. Wang, Q. Wang, N. Sun, S. Hu, S. Wei, H. Feng, X. Hao, W. Li, D. Kong, S. Wang, S. Chen, *Journal of Colloid and Interface Science* **2021**, 594, 604-620.

[8] K. Li, L. Han, J. Zhang, J. Cheng, *Small Struct.* **2023**, 2300210.

[9] L. Ma, S. Li, M. Yan, N. Gao, F. Liu, S. Ma, J. Xu, Y. Dai, E. Han, Z. Zhang, *Journal of Alloys and Compounds* **2023**, 949, 169847.

[10] S. Li, L. Ma, Z. Lei, *Carbon* **2022**, 186, 520-529.

Table S4. Comparison of peak of heat release rate and EMW performance of literatures.

Material	Minimum reflection loss (dB)	Peak of heat release rate(kW/m^2)
Fe-MOF-Rgo-EP 1	-43.6	554.1
CoC@FeNiG 2	-75.18	410.8
AgNC@BP/EP 3	-39.4	750.4
Hollow core-shell BCN@LDH/EP 4	-55.75	395.6
EP/Fe_3O_4-ppy nanocomposites 5	-35.7	443.8
MDCF@LDH/EP composite 6	-57.77	463.8
This work	-64.78	326.4

References

[1] Y. Li, Y. Li, B. Chen, W. Hu, D. Wang, *Journal of Alloys and Compounds* **2022**, 918, 165516.

[2] K. Li, L. Han, J. Zhang, J. Cheng, *Small Struct.* **2023**, 2300210.

[3] L. Xia, Z. Miao, J. Dai, A. Zhu, H. Xu, J. Zhong, Y. Chen, W. Luo, Y. Xu, C. Yuan, B. Zeng, H. Cao, L. Dia, *Chem. Eng. J.* **2022**, 438, 135402.

[4] Y. Qian, Y. Luo, Y. Li, T. Xiong, L. Wang, W. Zhang, S. Gang, X. Li, Q. Jiang, J. Yang, *Chem. Eng. J.* **2023**, 467, 143433.

[5] J. Guo, H. Song, H. Liu, C. Luo, Y. Ren, T. Ding, M. Khan, D. Young, X. Liu, X. Zhang, J. Kong, Z. Guo, *J. Mater. Chem. C.* **2017**, 5, 5334.

[6] Y. Qian, Y. Luo, A. Haruna, B. Xiao, W. Li, Y. Li, T. Xiong, Q. Jiang, J. Yang, *Small* **2022**, 18, 2204303.